PCCP

Accepted Manuscript

ROYAL SOCIETY OF CHEMISTRY

www.rsc.org/pccp

Formation of bcc and fcc during the coalescence of free and supported Fe and Ni clusters

Guojian Li, Qiang Wang*, Xudong Sui, Kai Wang, Chun Wu and Jicheng He

Key Laboratory of Electromagnetic Processing of Materials (Ministry of Education), Northeastern University, Shenyang 110819, China

Abstract

The formation of bcc and fcc during the coalescence of free and supported Fe and Ni clusters has been studied by molecular dynamics simulation using an embedded atom method. Structural evolution of the clusters, coalesced under varying temperature, Ni content and substrate conditions, was explored by interatomic energy, snapshot, pair distribution function and bond order parameters. The results show the formation of bcc and fcc is strongly related to Ni content, substrate and coalescence temperature. Free clusters coalesced at 1200 K form bcc at lower Ni contents with fcc forming at higher Ni concentrations and no observable coexistence of bcc and fcc. Differences in coalescence at 1000 K result from the coexistence of bcc and fcc within the Ni range of 50–70%. Free clusters supported on disordered Ni substrates were shown to transform from spherical morphology to islands of supported clusters with preferred epitaxial orientation. The Ni content required to form bcc and fcc coexistence on supported clusters at 1000 K decreased to 30%–50% Ni. Free clusters possessing coexistence of bcc and fcc generally stacked along the bcc (110) and fcc (111) facets, whereas supported clusters stacked along the (111) bcc and (100) fcc planes. Structural transformation was induced by clusters containing greater numbers of atoms. Spread over the substrate enhanced interatomic energy. Order substrates affect epitaxial growth direction and increase the melting points of the supported clusters. This study can be used to predict the nature of fcc and bcc formation in Fe-Ni films.

Keywords: cluster, Fe-Ni, coalescence, structural transformation, molecular dynamics simulation

1 Introduction

Magnetic films have attracted a wealth of attention as a result of their wide applications in the fields of magnetic recording, microelectromechanical systems (MEMS) and spintronic devices.[1] Fe-Ni films having high anisotropic magnetoresistance (AMR) properties, high saturation magnetization and low coercivity are one of the most important soft magnetic materials.[2–5] Magnetic properties of Fe-Ni films vary as a function of Ni content and can be further modified by changes in the surface morphology and microstructure of the films.[6,7] Structurally, Fe-Ni films exist as bcc, fcc and $L1_0$ depending on Ni content and result in differences to the films' magnetic properties.[8,9] Fe-Ni (fcc) films exhibit the highest

* Corresponding author. E-mail: wangq@mail.neu.edu.cn

magnetization values (1270 emu·cm^{-3}). The newfound $L1_0$-type Fe-Ni film has large uniaxial magnetic anisotropy energy.[10] Previous studies show that the formation of these structures is strongly related to the Ni content. However, the Ni content when forming fcc and bcc is different in Fe-Ni films when compared with the bulk. In bulk $Fe_{1-x}Ni_x$, bcc forms when x <0.26, whereas fcc forms at x values >0.34, with the coexistence of both fcc and bcc structures formed between these two compositions. Conversely, the Ni content required to form fcc or bcc structures in Fe-Ni films changes as a function of the preparation methods.[11] Therefore, designing structural variation in Fe-Ni films is necessary to tailor the required properties of the films for specific application.

The coalescence of free and supported clusters is prior to the formation of the continuous film during film growth. Therefore, there is a requirement to further understand the formation of bcc and fcc structures in coalesced Fe-Ni clusters with a function of Ni content to control the structural design of the films. As the coalescence process is complex,[12] computer simulation studies are required. Molecular dynamics (MD) simulation is an effective method to simulate the coalescence according to the accuracy and simulation scale. Regarding the coalescence of free clusters, significant attention has been paid to the coalescence of alloy clusters using MD simulation, such as Ag-Pd,[13] Au-Pt,[14] Cu-Ni[15] and Ni-Al.[16] For supported clusters, the melting and growth of pure metal clusters have been studied.[17–21] In these studies, it was found that the structural transformations of the free clusters—from fcc to icosahedron[17] or from decahedron to fcc[18]—varied when the clusters were supported on a substrate. The epitaxial growth is often achieved for supported clusters.[19,20] However, little attention has been paid to the structural formation of bcc and fcc structures during the coalescence of Fe-Ni clusters by MD simulation. Additionally, differences in the coalescence of free and supported clusters have not been studied.

In this study, MD simulation encompassing an embedded atom method was employed to simulate the coalescence of free and supported Fe and Ni clusters as a function of temperature. The correlation of bcc and fcc structures in the coalesced clusters resulting from the variation in Ni content, substrate conditions and coalescence temperature was then explored using snapshot, pair distribution function (PDF)[22] and the bond order parameter, W_6.[23] Finally, the formation reason of bcc and fcc during the coalescence is discussed.

2 Simulation details

The details of the MD simulation method are described in our previous studies.[24,25] In this study, the time-dependent interatomic energies of cluster fcc Ni_{531} were calculated by relaxing the cluster for 2 ns at 100 K with the time steps of 1.6, 2.0 and 4.0 fs. The results show that the energy curves with the time steps of 2.0 and 4.0 fs drift lower than that of 1.6 fs after relaxing for 0.5 and 1.0 ns, respectively. Therefore, a time step of 1.6 fs was used in this study. The embedded atom method (EAM) was used to describe the interatomic interaction of Fe-Ni.[26] In the EAM potential, the total energy can be described as

$$E = \frac{1}{2}\sum_{i,j,i\neq j}\phi_{ij}(r_{ij}) + \sum_{i}F_i(\rho_i) \quad (1)$$

where ϕ_{ij} and r_{ij} relate to the pair potential and distance between atoms i and j,

respectively, and F_i is the energy to embed an atom i into an electron density ρ_i, which can be calculated using

$$\rho_i = \sum_{j,j\neq i} f_j(r_{ij}) \tag{2}$$

where f_j is the electron density of atom i arising from atom j and can be written as

$$f(r) = \frac{f_e \exp[-\beta(\frac{r}{r_e}-1)]}{1+(\frac{r}{r_e}-\lambda)^{20}} \tag{3}$$

To proceed with a smooth variation of the embedding energy, the embedding energy functions are divided as follows:

$$F(\rho) = \begin{cases} \sum_{i=0}^{3} F_{ni}(\frac{\rho}{\rho_n}-1)^i, \rho < \rho_{\mathrm{n}}, \rho_{\mathrm{n}} = 0.85\rho_e \\ \sum_{\mathrm{i}=0}^{3} F_i(\frac{\rho}{\rho_e}-1)^i, \rho_{\mathrm{n}} \le \rho < \rho_o, \rho_{\mathrm{o}} = 1.15\rho_e \\ F_e\left[1-\ln\left(\frac{\rho}{\rho_e}\right)^{\eta}\right]\cdot\left(\frac{\rho}{\rho_e}\right)^{\eta}, \rho_{\mathrm{o}} \le \rho \end{cases} \tag{4}$$

In addition, the pair potentials have the form

$$\phi(r) = \frac{A\cdot\exp[-\alpha(\frac{r}{r_e}-1)]}{1+(\frac{r}{r_e}-\kappa)^{20}} - \frac{B\cdot\exp[-\beta(\frac{r}{r_e}-1)]}{1+(\frac{r}{r_e}-\lambda)^{20}} \tag{5}$$

where r_e is the equilibrium distance of the nearest neighboring atoms. A, B, α, β, κ and λ are adjustable parameters. For an alloy system, the alloy pair potential of atoms *a* and *b* is defined using the alloy model

$$\phi^{ab}(r) = \frac{1}{2}\left(\frac{f^b(r)}{f^a(r)}\phi^{aa}(r) + \frac{f^a(r)}{f^b(r)}\phi^{bb}(r)\right) \tag{6}$$

The parameters of the EAM potential needed to define Fe and Ni are listed in Table 1.

Table 1. EAM parameters.

	Fe	Ni
r_{e}	2.481987	2.488746
f_{e}	1.885957	2.007018
ρ_{e}	20.041463	27.984706
α	9.818270	8.029633

β	5.236411	4.282471
A	0.392811	0.439664
B	0.646243	0.632771
κ	0.170306	0.413436
λ	0.340613	0.826873
F_{n0}	-2.534992	-2.693996
F_{n1}	-0.059605	-0.066073
F_{n2}	0.193065	0.170482
F_{n3}	-2.282322	-2.457442
F_0	-2.54	-2.70
F_1	0	0
F_2	0.200269	0.282257
F_3	-0.148770	0.102879
η	0.391750	0.509860
F_e	-2.539945	-2.700493

The accuracy of the EAM during simulation of Fe-Ni alloys was justified by comparing the simulated phase diagram of bulk Fe-Ni with the experimental results,[27] as shown in Fig. 1. The setup of the bulk Fe-Ni extended from a $7a_0 \times 7a_0 \times 7a_0$ cubic periodic super cell with an fcc structure possessing 1372 atoms and a bcc structure including 1241 atoms. The liquidus curve was determined as a function of the melting points of bulk Fe-Ni materials with varying Ni content. Melting points were obtained by the sharp increase of energy with temperature. The melting processes were calculated by heating the bulk materials from 1000 to 3800 K in 100 K incremental steps and equilibrated at each temperature for 0.3 ns. As the temperature approached the melting point, the incremental temperature steps were reduced to 10 K for a shorter equilibrated time to maintain a constant heating rate. As is evident from Fig. 1, the melting points of bulk Fe-Ni materials are affected by the original structures. The melting point of fcc original structure are higher that of bcc original structure at the same Ni content. The simulated melting point of bulk bcc Fe is about 1200 K higher than the experimental value and that of bulk fcc Ni is about 840 K higher than the experimental value. This is because there is no free surface for the simulation of the periodic bulk.[28] Furthermore, the contribution of surface energy of Fe (2206 mJ/m^2) is higher than that of Ni (2104 mJ/m^2),[29] which leads to the difference between the simulated and experimental values of Fe is higher than that of Ni. The variation trend of simulated melting points with the Ni content can be compare with the experimental results by adjusting the y-axis to make the experimental melting points of bcc Fe and fcc Ni overlap with the corresponding simulated values, as shown in Fig. 1. Clearly, when the original structure is bcc (Ni $\leq$30%), they agree well. The experimental values are between the melting points of bcc and fcc for 40% < Ni <80% due to the coexistence of bcc and fcc between these Ni compositions. When the Ni value >90%, their trends are consistent. Thus, it is reasonable to assume the simulated results are consistent with the experimental results. The consistency indicates that the EAM potential can be used to describe the interaction of Fe and Ni.

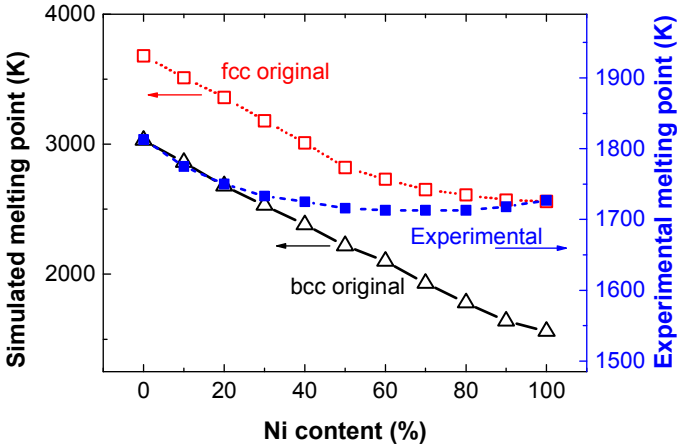

Fig. 1. Simulated liquidus curve data of bulk Fe-Ni with fcc and bcc original structures compared with the corresponding experimental results.

The coalescence construction of Fe and Ni clusters is shown in Fig. 2. The total atomic number of the coalesced clusters is 531. Ni content was tuned by varying the size ratio of the clusters with respect to Fe and Ni. The atomic number ratios of Fe to Ni are 478 : 53 (10% Ni), 372 : 159 (30% Ni), 266 : 265 (50% Ni), 159 : 372 (70% Ni) and 53 : 478 (90% Ni), respectively. The Fe and Ni clusters with varying sizes were obtained by cutting directly from their corresponding bulk $30a_0 \times 30a_0 \times 30a_0$, where a_0 represents the bulk lattice constant. Thus, the original structures of Fe and Ni are bcc and fcc, respectively. These clusters were annealed by relaxing for 0.2 ns at 600 K and further cooled to 300 K. In this study, for all cooling processes, the incremental temperature step is 50 K with relaxation times of 0.2 ns. For the coalesced clusters, the annealed Fe and Ni clusters were placed within the center of a $30a_0 \times 30a_0 \times 30a_0$ box having a periodical boundary condition, as shown in Fig. 2. For supported clusters, the difference was that the Fe and Ni clusters were supported on a $30a_0 \times 30a_0 \times a_0$ Ni substrate. The Ni substrate was used to avoid lattice distribution effects between the cluster and the substrate during structural evolution. The Ni substrate was composed of two fixed disorder layers to avoid any deformation and epitaxial growth. To compare the effects of varying substrate parameters, three other substrate conditions were also simulated, namely the three fixed (110) layers, three fixed (111) layers and four free (100) layers residing on two fixed (100) layers.

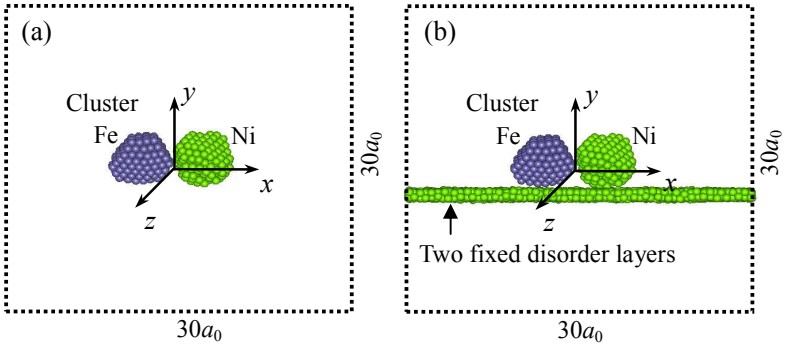

Fig. 2. Coalescence construction of (a) free and (b) supported Fe and Ni clusters.

The coalescence temperatures were selected according to the melting points of the mixed 531 atom Fe-Ni clusters with varying Ni content. As there are two crystal structures, bcc and fcc, in the Fe-Ni alloys, depending on Ni content, the melting point of mixed clusters with both bcc and fcc original structures was calculated by heating the clusters to 1600 K—above all cluster melting points—from 300 K with incremental temperature steps of 20 K and relaxation times of 0.2 ns for each individual step. Melting points of the Fe-Ni clusters as a function of Ni content and their original crystal structures are shown in Fig. 3. It is evident from the data that the melting points of the clusters decrease with increasing Ni content. The original structures of bcc and fcc have no significant effect on the melting points. The reason for this relates to the fact that the structures of the clusters change to bcc at lower Ni contents and to fcc at higher Ni contents after relaxation for 0.2 ns at 300 K irrespective of whether the initial structure is fcc or bcc. According to the fitted curve of the melting points, 1200 K and 1000 K were selected as the coalescence temperatures. At 1200 K, the clusters coalesce as solids for lower Ni contents (10–30% Ni) and as liquids for higher Ni contents (50–90% Ni). At 1000 K, all clusters are solid across the entire Ni content range. The coalesced clusters with varying Ni content were coalesced for 0.5 ns at the coalescence temperatures prior to further cooling to 300 K. The structures and morphologies of the coalesced clusters were thereafter analyzed by snapshot, PDF and the bond order parameter, W_6.

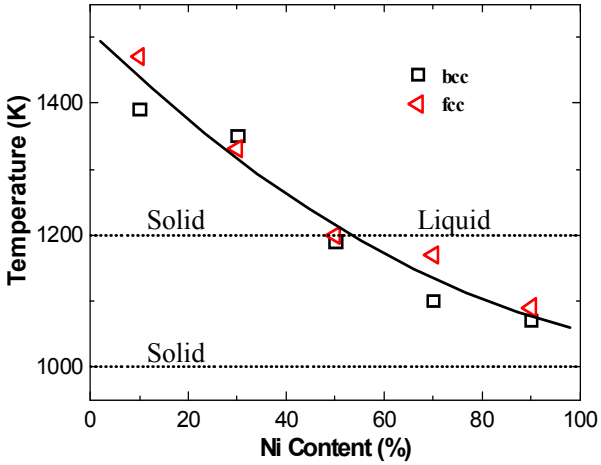

Fig. 3. Melting points of the mixed Fe-Ni clusters as a function of Ni content together with their initial crystal structures. The solid line represents the fitting curve of the melting points. The dotted lines show the coalescence temperatures, which predict whether the coalesced clusters remain in the solid or liquid state.

3 Results and discussion

The temperature-dependent interatomic energies of the free clusters during the cooling processes are used to confirm the state of the coalesced clusters at the selected coalescence temperature. Since the melting behavior of transition metals, such as Pd, has been shown to be heating-rate dependent,[30,31] the interatomic energies of the free clusters with different cooling rates are also considered. The cooling rates are represented by the equilibrium time at

each temperature. In this study, equilibrium times of 0.1 (500 K/ns), 0.2 (250 K/ns) and 0.5 ns (100 K/ns) were studied. The temperature-dependent interatomic energies of the free coalesced clusters as a function of Ni content and equilibrium time are shown in Fig. 4. Clearly, there is a significant reduction in the interatomic energy with decreasing temperature for clusters with 50–90% Ni content for the three cooling rates. The interatomic energies of clusters containing 10% and 30% Ni decrease linearly as a function of decreasing temperature; 1200 K is higher than the melting points of the clusters that possess 50–90% Ni, meaning that the three clusters of higher Ni content were in the liquid state at 1200 K and solidification occurred during the cooling processes. The abrupt change of latent heat occurs for these three clusters; however, the clusters with 10% and 30% Ni remain solid—thus, no solidification or an abrupt change of latent heat appears. The significance of the data means that the selected coalescence temperatures are appropriate and can form coalescence of the clusters either in the solid or liquid states. Additionally, it is also evident that the long equilibrium times have no significant effect on the interatomic energy for clusters with 10% and 30% Ni (Fig. 4d). However, for clusters possessing 70% Ni, the long equilibrium time allows the cluster to remain in a low-energy state. The variation of equilibrium time has little effect on the crystal structures for the free coalesced clusters. Hence, further studies only consider equilibrium times of 0.2 ns.

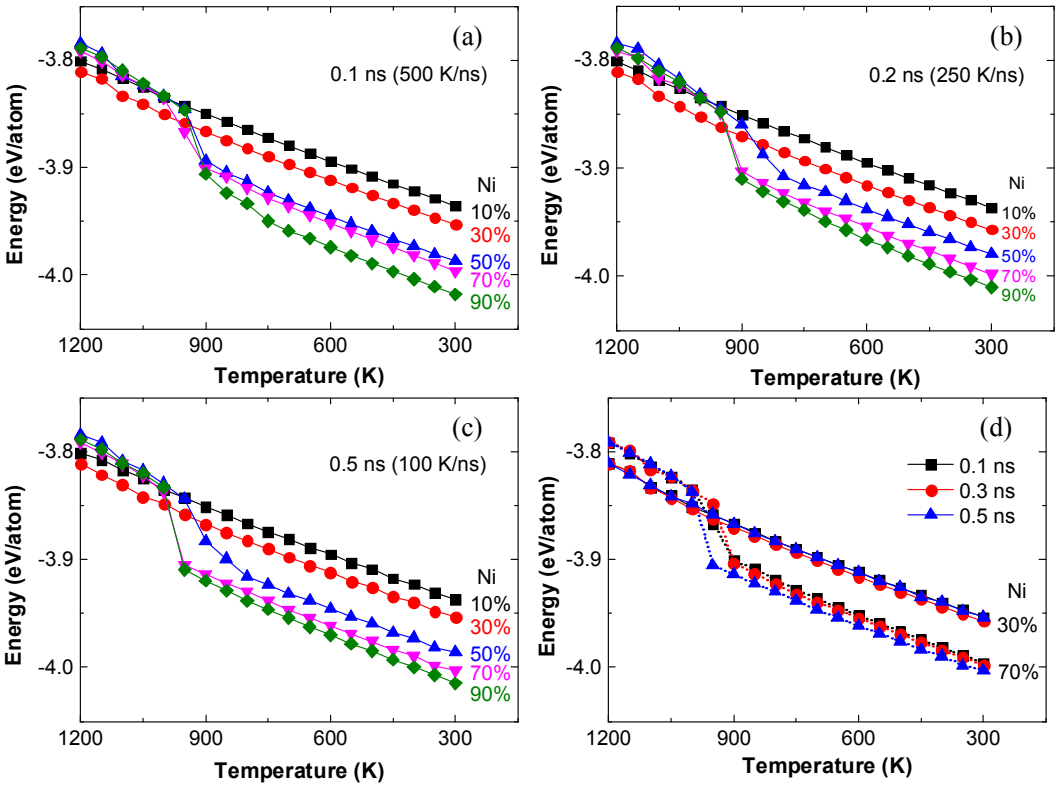

Fig. 4. Temperature-dependent interatomic energies of the free coalesced clusters as a function of Ni content during the cooling processes. The equilibrium times at each temperature vary: (a) 0.1 ns (500 K/ns), (b) 0.2 ns (250 K/ns) and (c) 0.5 ns (100 K/ns). (d) is the comparison of (a)–(c) containing 30% and 70% Ni.

Fig. 5 provides snapshots at 300 K of the coalesced clusters with varying Ni content and coalescence temperatures. As observed, the morphologies of the coalesced clusters differ. Spherical morphology was formed at 1200 K whereas ellipsoids were formed at 1000 K. The coalesced clusters with 10% and 30% Ni possess stacking features relating to (110) facets. The rectangular atomic arrangement of the (110) facet corresponds to the (110) bcc structure and all four coalesced clusters formed the bcc structure. The two coalesced clusters with 50% and 70% Ni were composed of five (111) facets at 1200 K possessing decahedron morphology. However, the configurations of the clusters with 50% and 70% Ni coalesced at 1000 K are different to the cases at 1200 K. A portion of the Ni and Fe atoms did not coalesce, instead retaining their initial structures. This leads to the coexistence of fcc and bcc structures in the two clusters. The quantity of bcc for the coalesced cluster with 70% Ni is less than the corresponding cluster containing 50% Ni. The atomic arrangement of the (111) facets, stacked to form the coalesced clusters with 90% Ni, relates to hexagonal fcc, meaning that the coalesced cluster with 90% Ni formed an fcc structure. For the cluster with 70% Ni, the facet was formed by two parts of the hexagonal fcc Ni and the rectangular bcc Fe. Clusters with bcc and fcc coexistence were defined by bcc (110) and fcc (111) stacked facets. Additionally, hexagonal morphology is formed for such coalesced clusters. Furthermore, similar morphology is easily obtainable for non-supported, free clusters. Previous studies have proven this phenomenon,[18,32,33] suggesting that as the hexagonal configuration is similar to the closed-packing plane, the free energy of the system decreases.

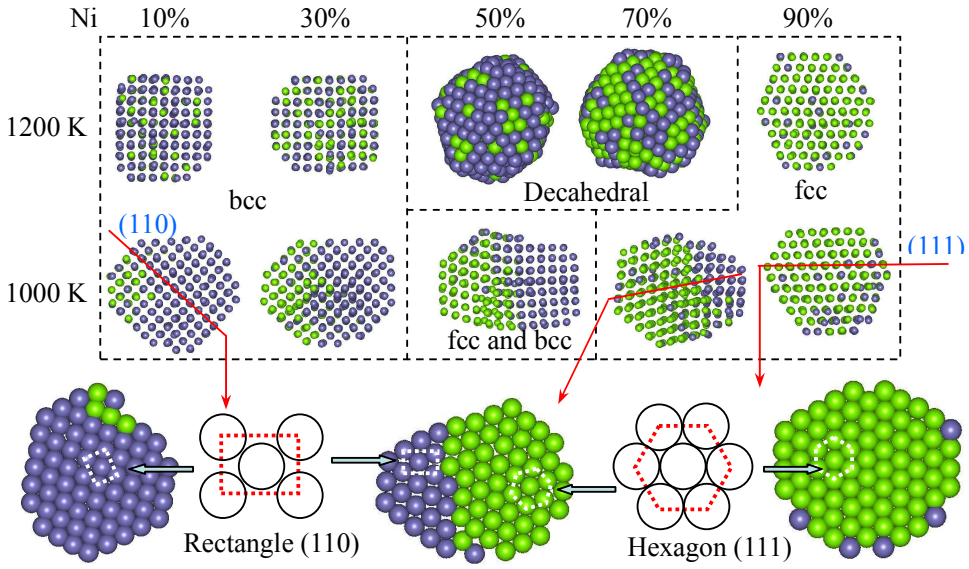

Fig. 5. Snapshots at 300 K after cluster coalescence as a function of Ni content at varying temperatures followed by cooling to 300 K. The bottom row displays atomic arrangements of the bcc (110) and fcc (111) facets of sliced clusters.

PDFs were used to define the crystal structures of the coalesced clusters, as shown in Fig. 6. The standard peaks of bcc and fcc are shown by their respective dotted lines. Clearly, the peaks of the coalesced clusters possessing 10% and 30% Ni at 1200 K relate to the bcc structure. When increasing the Ni content to 50%, the majority of the peaks correspond to fcc stacking with the presence of only one weak peak relating to bcc appearing at 0.28 nm. In clusters containing

70–90% Ni, only fcc peaks appear. That is to say, the coalesced clusters with higher Ni contents form an fcc structure. For the clusters coalesced at 1000 K, the results are similar to those of the clusters formed at 1200 K. The only difference is within the coalesced cluster possessing 50% Ni, which exhibits significant characters of both fcc and bcc stacking. For the coalesced cluster containing 70% Ni, a weak peak corresponding to bcc stacking appears at 0.28 nm. These PDF data are complementary to the results of the snapshots.

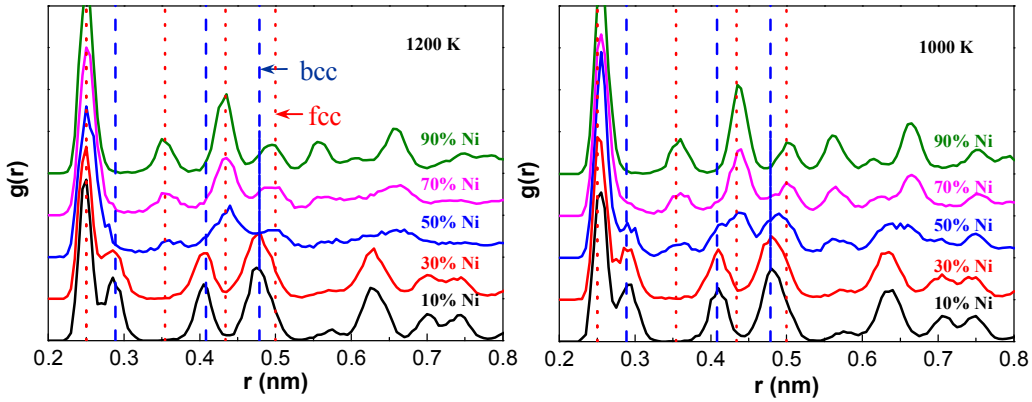

Fig. 6. Pair distribution functions at 300 K after cluster coalescence as a function of Ni content at different temperatures followed by cooling to 300 K. The standard peaks relating to bcc and fcc are shown by their respective dotted lines.

The bond order parameter, W_6, was used to confirm the cluster structures to a higher degree of accuracy as W_6 is less sensitive to the neighboring environment in close proximity.[34] As shown in Fig. 7, by comparison to the standard W_6 values of bcc, fcc and decahedron, bcc stacking formed for the coalesced clusters containing 10% and 30% Ni at 1200 K and 1000 K. Decahedron formation within the coalesced clusters possessing 50% and 70% Ni at 1200 K is shown. The fcc structure was formed within the coalesced cluster composed of 90% Ni at 1200 K and 1000 K. The W_6 value of the cluster with 50% Ni at 1000 K is between the values of bcc and fcc, confirming the coexistence of both bcc and fcc stacking in the cluster. The W_6 value of the cluster containing 70% Ni is a little higher than that of the standard fcc value, suggesting that fcc was preferentially formed with the coexistence of bcc as a minor phase. All results are in agreement with those of the PDF data. Hence, the PDF model is a useful tool to confirm the crystal structure of the coalesced clusters.

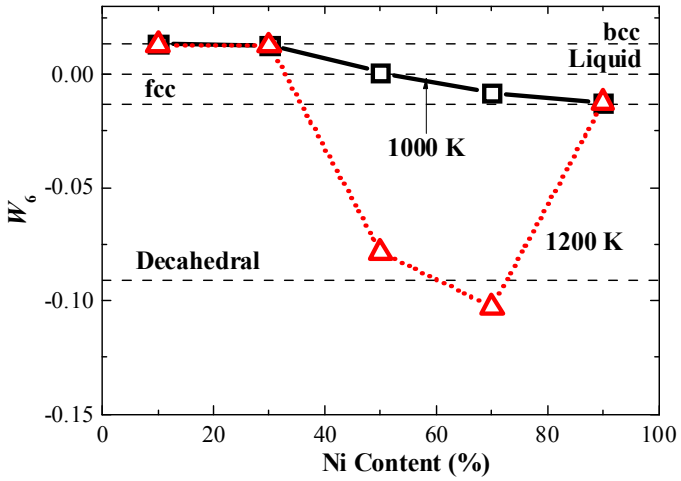

Fig. 7. Bond order parameter, W_6, values at 300 K after cluster coalescence with different Ni content at different temperatures followed by cooling to 300 K. The standard values of bcc, liquid, fcc and decahedral structures are represented by their respective dotted lines.

Fig. 8 depicts the snapshots at 300 K of the supported clusters coalesced at 1200 K and 1000 K, viewed from different angles. For clarity, some substrate atoms are shown in dots in the figure. It is evident that the morphologies of the supported coalesced clusters are significantly different to the free clusters (Fig. 5). Preferred growth—similar to Co clusters on Cu (001) surfaces[35]—also occurs to some extent despite the presence of the disordered substrate. Islands form for all supported clusters. Observation from the side view shows stacked islands by atomic layers. At 1200 K, the atomic layers reduce from nine at 10% Ni composition to three layers when increasing the Ni content to 90%. Viewing from the top shows that the atomic layer shape is almost square in nature. Growth in the first (bottom) atomic row layer of the supported clusters is observed as the clusters possess 20 rows at 90% Ni content up from 11 rows at 10% Ni content. At 1000 K, the reduction of layer numbers and enhancement of atomic rows in the bottom layer with increasing Ni content is not as pronounced as the clusters formed at 1200 K, indicating that both the coalescence temperature and Ni content have a significant effect on the configuration of the coalesced islands. At higher temperatures, atoms are subjected to higher energy and are able to diffuse on the surface of the substrate. The use of snapshots without other complementary models gives rise to difficulties in accurately obtaining the crystal structure of the supported coalesced clusters.

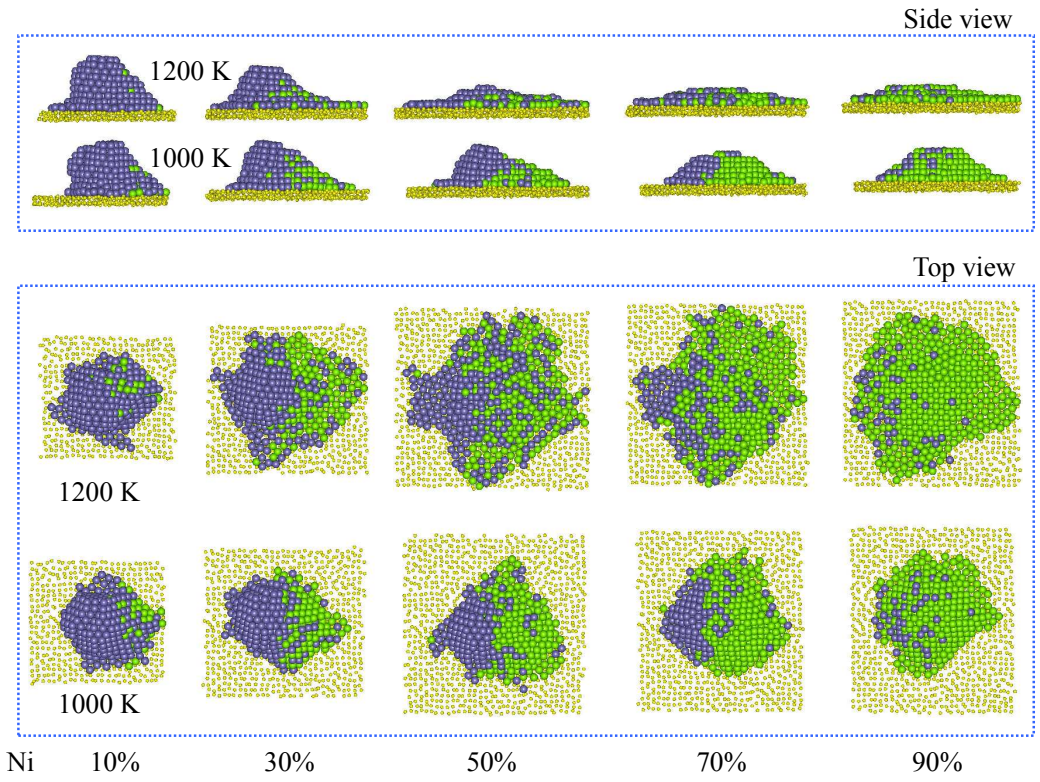

Fig. 8. Snapshots at 300 K of supported coalesced clusters as a function of Ni content and coalescence temperature, viewed from different angles. The lower dots represent the substrate atoms.

PDFs were then used to define the crystal structures of the supported clusters, as shown in Fig. 9. At 1200 K, the peaks of the clusters possessing 10% and 30% Ni content exhibit obvious bcc character. For clusters containing higher Ni content, the enhanced spread of the atomic layers within the supported clusters means that the substrate effect on their crystal structures becomes more significant. This leads to the appearance of multiple low-intensity peaks. However, the main peaks correspond to those of fcc. Similar findings occur for clusters coalesced at 1000 K. Here, clusters composed of 70% and 90% Ni have significant fcc character—the substrate effect on the crystal structure decreases. For the cluster possessing 10% Ni content, the structure is clearly bcc. Increasing the Ni content in the cluster to 30% and 50%, the stacking character becomes ambiguous as the bcc character also displays weak signs of fcc structure, meaning a coexistence of both bcc and fcc structures in the clusters. Typically, fcc stacking appears at lower Ni contents for supported clusters. The reason is discussed below. Lattice constants were calculated from the first PDF peaks and calculated as 0.294 nm and 0.361 nm for free bcc and fcc clusters, respectively. The corresponding values for the supported clusters increased to 0.323 nm (bcc) and 0.396 nm (fcc) because of the presence of the substrate effect. This leads to the shift in the spectra with respect to r (nm) as the bcc and fcc markers shift in (in Figure 6).

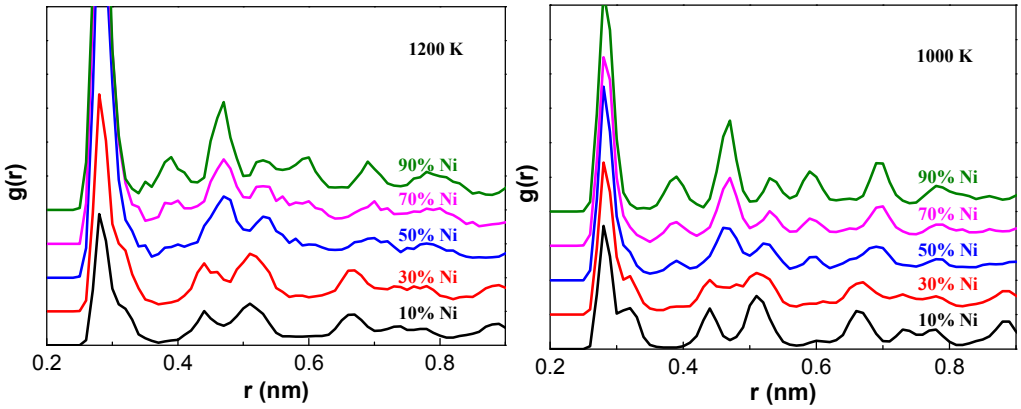

Fig. 9. Pair distribution functions at 300 K of coalesced supported clusters as a function of Ni content at different temperatures followed by cooling to 300 K.

This study found that the disordered substrate failed to suppress preferred growth of the supported clusters. To clarify the structure of the supported coalesced clusters, their structural details at 300 K are explored for clusters composed of 30% and 70% Ni at 1000 K. The structure of the 30% Ni cluster shows the presence of bcc and fcc coexisting, whereas the character is solely fcc for the cluster possessing 70% Ni. The atomic arrangements between different layers of the supported clusters are shown in Fig. 10. It is discernible that the coalesced islands are formed by five facets for both Ni compositions as viewed from the top. The four side facets are constructed from (111) crystallographic planes. The bottom layer, contacted with the substrate, is shown in addition to the surface layer. The atomic arrangements differ between the two Ni compositions even though they are coalesced on the same substrate. For the 30% Ni cluster, the arrangement of the Ni atoms relates to the (100) fcc plane, whereas the corresponding Fe atoms arrange in the (111) bcc plane. At the Fe-Ni interface, a portion of the Fe atoms are arranged parallel to the (100) fcc plane; however, no Ni atoms stack within the (111) bcc plane. In relation to the surface layer, the atomic arrangement is that of the (111) bcc plane—the reason for the coexistence of bcc and fcc in the clusters composed of 30% Ni. For the corresponding 70% Ni cluster, the stacking of both the Ni and Fe atoms in the bottom layer is within the (100) fcc plane. Fe atoms were induced by the presence of Ni atoms to arrange along the (100) fcc plane, indicating that significant structural transformation was induced by the Ni atoms. The stacking of the surface layer within the cluster corresponds to the (100) fcc plane. In this study, the bcc structure on the substrate stacks along its (111) plane, whereas the fcc structure stacks along its (100) plane. Furthermore, the formation of the coexistence of the bcc and fcc structures on the supported clusters differs from the results of the corresponding free clusters, which stack along the bcc (110) and fcc (111) facets, while the supported clusters stack along the bcc (111) and fcc (100) facets. The existence of stacking along the (111) facets of both the fcc and bcc structures did not appear.

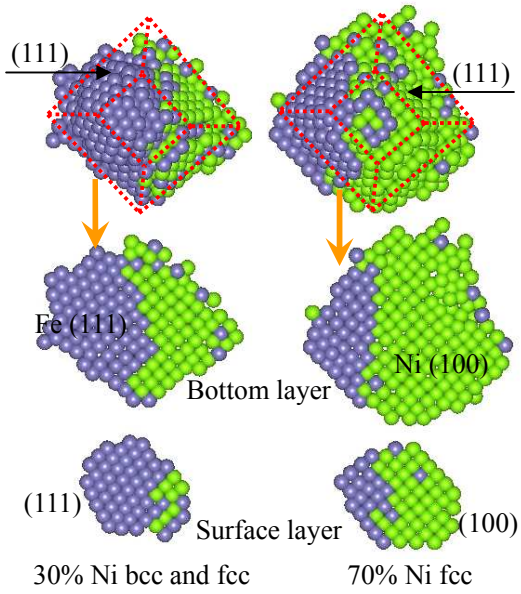

Fig. 10. Atomic arrangements of the supported coalesced clusters with varying Ni content coalesced at 1000 K followed by cooling to 300 K.

The formation reason of the fcc and bcc structures as a function of Ni content was studied by calculating the interatomic energies of the mixed clusters at 0 K with the original fcc and bcc structures. The results are shown in Fig. 11. As observed, the interatomic energies of the supported clusters are lower than the corresponding free clusters with the same Ni content and original structure. The significance is that the supported clusters are more stable than that of the free clusters. Similar results found that the structural stability of the supported cluster was enhanced through the interaction of the cluster with the substrate.[17] The interatomic energy decreases with increasing Ni content. Regarding the free clusters, the bcc structure is more stable than that of the fcc structure at lower Ni contents, whereas the fcc structure becomes stable at higher Ni contents. In relation to the supported clusters, a similar trend is observed; however, the stability of the fcc structure occurs at lower Ni contents, indicating that the fcc structure is more stable on the supported clusters than that of the free clusters, leading to the presence of fcc structures at Ni concentrations of 30% (Fig. 9) for the supported clusters and 50% (Fig. 6) for the free clusters.

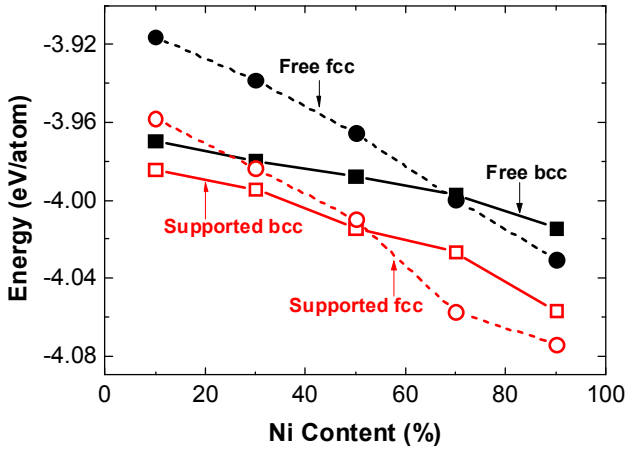

Fig. 11. Cluster interatomic energies as a function of Ni content and their original crystal structures after relaxing for 0.5 ns at 0 K.

The interatomic energies during the cooling processes for the supported clusters coalesced at 1200 K and 1000 K are shown in Fig. 12. It can be seen that the interatomic energies linearly decrease with decreasing temperature when the clusters coalesced at 1000 K. Furthermore, the interatomic energies decrease with increasing Ni content at the same temperature, similar to the results of the free clusters. However, at 1200 K, the variation of interatomic energies displays a different trend to that at 1000 K. The energies increase with decreasing temperature in the range of 1200–1000 K, except for the cluster containing 10% Ni. Additionally, the atomic energies increase with increasing Ni content at the same temperature. By observing differences in the structures of the clusters between 1200 K and 1000 K, it was found that cluster height decreases and the atoms spread over a greater area on the substrate. For the cluster containing 10% Ni, this phenomenon is not significant, suggesting that the atomic diffusion on the substrate increases the energies as the temperature decreases.

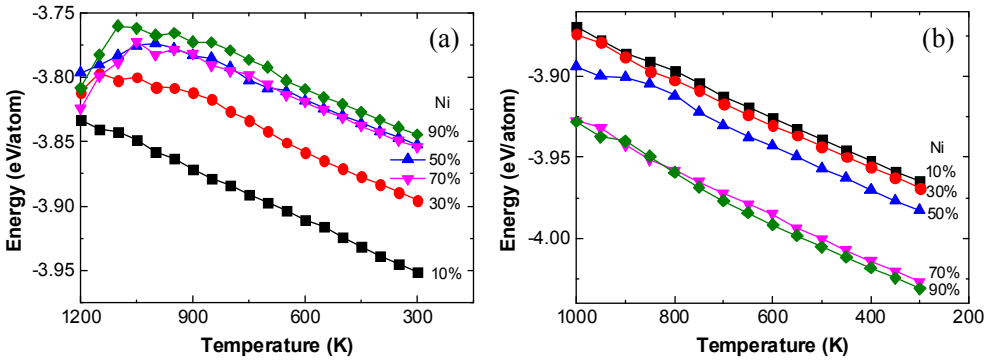

Fig. 12. Temperature-dependent interatomic energies of the supported coalesced clusters with varying Ni content during the cooling processes. (a) 1200 K and (b) 1000 K.

Additionally, differences in interatomic energies were calculated by using the energy at 300 K of free coalesced cluster subtract that of supported coalesced cluster and are shown in Fig.

13. The positive value of energy difference expresses the supported clusters are more stable than that of free clusters. As observed, the value of energy difference at 1000 K is positive, signifying that the presence of the substrate stabilizes the cluster. A similar case occurs for the supported coalesced cluster having 10% Ni at 1200 K. However, when increasing the Ni content beyond 10%, the value of the energy difference becomes negative. That is to say, the energy of the supported cluster increases. Furthermore, such enhancement significantly increases as a function of increasing Ni content. This phenomenon is related to the area of the atomic spread on the substrate, with greater spread in the substrate leading to enhanced interatomic energy.

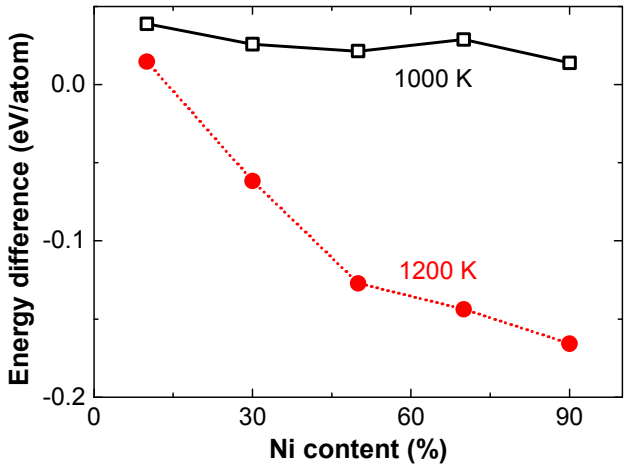

Fig. 13. Differences in interatomic energies for free and supported coalesced clusters at 300 K.

It is a well-known phenomenon that the surface effect is enhanced in the presence of small clusters. To justify structural variations as a function of the surface effect, the coalescence of the large clusters at varying coalescence temperatures was simulated. The large cluster includes 1062 atoms with a Ni content of 50% as the coexistence of bcc and fcc structures appears under such conditions. The morphologies and crystal structures were primarily studied by complementary snapshots and PDFs, as shown in Figs. 14 and 15, respectively. The morphologies and the coexistence of bcc and fcc structures within the large clusters at the coalescence temperatures in the presence of the substrate are similar to those of the small clusters. However, a significant size effect is also exhibited. At 1200 K, the alloying of Fe and Ni atoms becomes ambiguous for the large coalesced clusters, attributed to the atoms in the large cluster lacking sufficient energy to diffuse at 1200 K. Additionally, since the melting temperature of Ni clusters is lower than that of Fe, the majority of Fe atoms still aggregate together at 1200 K, while Ni atoms will have already spread on the substrate. At the lower temperature of 1000 K, the results are similar to the small clusters. With respect to the PDF data, the most significant change comes from stronger peak intensity when compared with the small clusters because of the increased cluster size. When comparing this with the results of the corresponding small clusters, the coexistence of bcc and fcc structures becomes significant, especially for the free clusters at 1200 K.

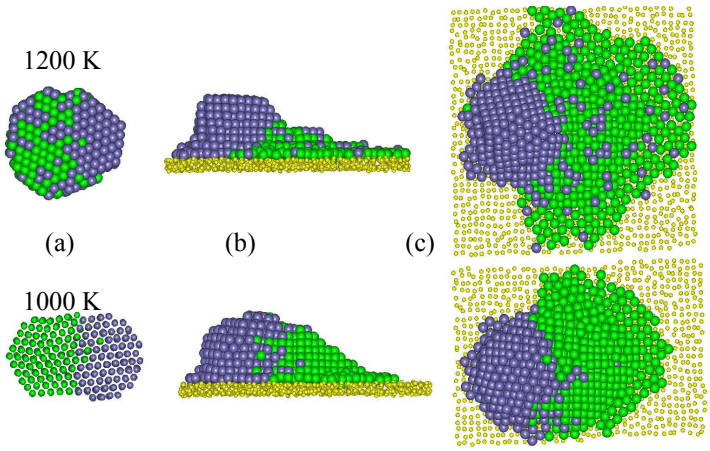

Fig. 14. Snapshots of coalesced clusters at 300 K with 1062 atoms and 50% Ni coalesced at 1200 K and 1000 K for (a) free clusters and (b) supported clusters from side view and (c) top view.

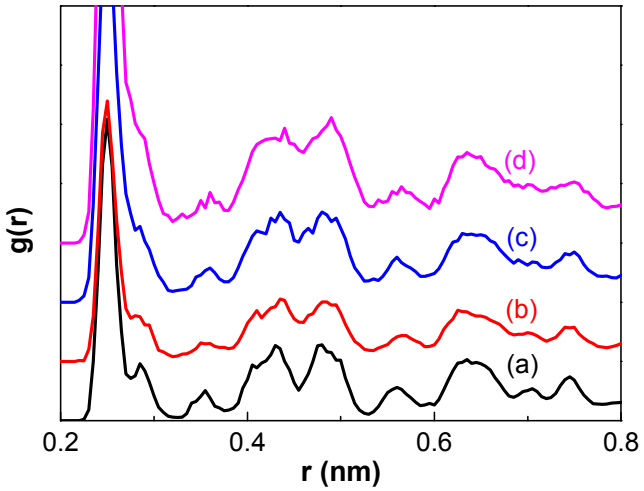

Fig. 15. Pair distribution functions of coalesced clusters at 300 K for free clusters coalesced at 1000 K (a) and 1200 K (b) and supported clusters coalesced at 1000 K (c) and 1200 K (d). The standard peaks of bcc and fcc are also shown by their respective dotted lines.

To define the effects of varying substrate conditions on the coalescence, clusters coalesced on free (100), fixed (110) and fixed (111) substrates were simulated. The PDFs, interatomic energies as a function of temperature and snapshots were calculated to analyze how varying parameters of supported substrates affect the resulting structures. The snapshots at 300 K of supported clusters with 50% Ni coalesced at 1200 K and 1000 K are shown in Fig. 16. The morphologies are significantly different upon changes to the substrate conditions. Additionally, the coalescence temperature also affects morphology; however, the substrate conditions have a greater impact than that of the coalescence temperature. Atoms in the coalesced clusters show epitaxial growth on all ordered substrates. For the free (100) substrate, a portion of the atoms embed into the substrate, increasing with temperature. Additionally, the height of the coalesced islands decreases with increasing coalescence temperature, while

alloying of Fe and Ni atoms occurs to a greater extent at 1200 K than at 1000 K.

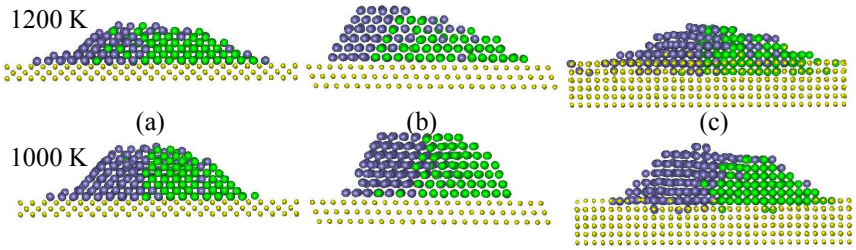

Fig. 16. Snapshots at 300 K of supported clusters with 50% Ni coalesced at 1200 K and 1000 K on (a) fixed (110), (b) fixed (111) and (c) free (100) Ni substrates. The lower dots represent the substrate atoms.

PDFs were calculated to analyze the crystal structures of the coalesced clusters supported on varying substrates (Fig. 17) as snapshots alone are not able to reflect the details. The main difference between the fcc and bcc structures is in their peak positions. One peak of bcc appears at 0.45 nm and that of fcc appears at 0.39 nm. Clearly, all the clusters exhibit the characters of both fcc and bcc when subjected to the given coalescence temperatures and substrate conditions, meaning that the coexistence of fcc and bcc is unaffected by the substrate conditions. According to the above morphologies, the atomic arrangements possess order on the three substrates under the simulated conditions; however, peak intensities differ—the reason being that PDFs present probabilities of finding a pair of atoms with a distance r in a layer. The supported coalesced clusters form islands with varying atomic alignments, leading to discrepancies in peak intensity.

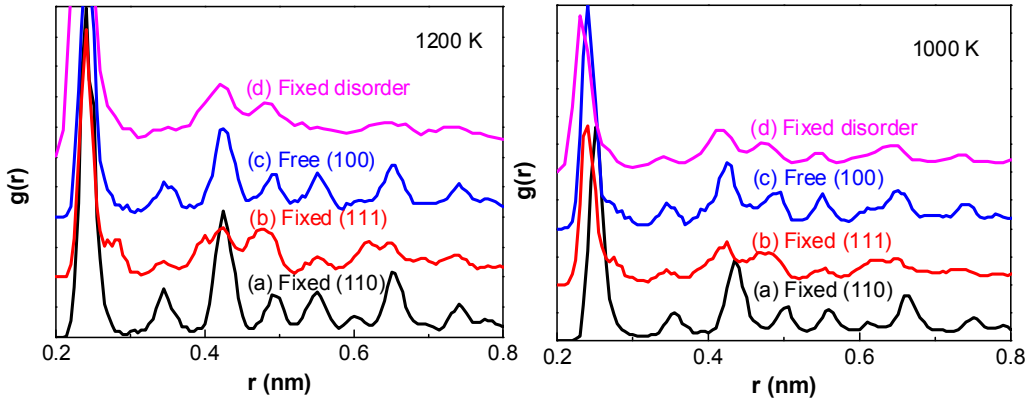

Fig. 17. Pair distribution functions of coalesced clusters at 300 K for supported clusters coalesced at 1200 K and 1000 K on (a) fixed (110), (b) fixed (111) (c) free (100) and a fixed disordered Ni substrate.

Interatomic energies of the supported clusters containing 50% Ni during the cooling processes after coalescing at 1200 K on fixed disordered, fixed (110), free (100) and fixed (111) Ni substrates were calculated to determine the stability of the supported coalesced clusters (Fig. 18). The cluster supported on the fixed (111) substrate has the lowest energy at 300 K. As a function of substrate interatomic energy increases in the order: free (100) < fixed (110) < fixed disordered. Therefore the (111) substrate allows stabilization of the structures.

Clusters also become stable when supported on the free (110) substrate as in this case the atoms embed into the substrate. There is a significant increase of the interatomic energy for clusters supported on the fixed disordered substrate and the primary difference in their structures is that the height of the clusters reaches four atomic layers compared with six atomic layers for the other substrates. Additionally, for all four substrate cases, there is an absence of latent heat as epitaxial growth occurs at 1200 K for clusters supported on fixed (110), free (100) and fixed (111) substrates. This signifies that the coalesced clusters had not melted at 1200 K and thus the substrates increase the melting points as found in previous studies.[17,18] Melting of the supported coalesced clusters containing 50% Ni was simulated. The results indicate that aligned clusters' melting points significantly increased on fixed substrates. The melting points of the clusters on fixed (110), free (100) and fixed (111) Ni substrates are 1600 K, 1400 K and 1700 K, respectively. All supported clusters possess higher melting points than corresponding free clusters (1200 K). Furthermore, the free (100) cluster has the lowest melting point, indicating significant influence as a function of the substrate condition.

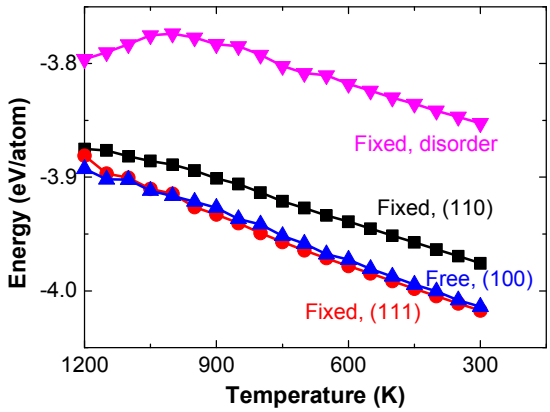

Fig. 18. Interatomic energies of supported clusters containing 50% Ni during the cooling processes after coalescing at 1200 K on fixed disordered, fixed (110), free (100) and fixed (111) Ni substrates.

4 Conclusions

In this study, MD simulation using an embedded atom method was employed to simulate the coalescence of free and supported Fe and Ni clusters. The effects were studied as a function of Ni content, coalescence temperature and substrate conditions to clarify the formation of bcc and fcc. The results indicated that the formation of bcc and fcc significantly differs for the free and supported clusters when subjected to varying temperatures, substrate conditions and Ni content. Regarding the free clusters, bcc formed at 10% and 30% Ni, whereas fcc formed at 50–90% Ni at 1200 K. There was no evidence of the coexistence of bcc and fcc. At 1000 K, the main observable difference was in the coexistence of bcc and fcc within the Ni range of 50–70%. Supporting the clusters on disordered Ni substrates resulted in the free clusters coalescing to form spheres, whereas the supported clusters formed islands with preferred epitaxial growth to some degree despite the presence of a disorder substrate. Furthermore, at

1000 K, the Ni content required to form the fcc structure reduced to 30% and 50% compared with the results of free clusters. Additionally, the free clusters exhibiting coexistence of both bcc and fcc stacking possessed bcc (110) and fcc (111) facets, while the supported clusters stacked along the (111) bcc plane and (100) fcc plane. The structural transformation was induced by larger clusters containing greater numbers of atoms. The atoms spread over the substrate and increased the interatomic energy. The substrate conditions affected the interatomic energies and also increased the melting points. This study indicates that the formation of fcc and bcc can be tuned by the coalescence temperature, substrate and Ni content, providing a method to tune the fcc and bcc structures of Fe-Ni films.

Acknowledgements

This work was supported by the National Natural Science Foundation of China (Grant Nos. 51425401 and 51101034) and the Fundamental Research Funds for the Central Universities (Grant Nos. N130509002 and N140902001).

References

1 P. J. Jensen and K. H. Bennemann, *Surf. Sci. Rep.*, 2006, **61**, 129–199.
2 H Kuru, H. Kockar, M. Alper and O. Karaagac, *J. Magn. Magn. Mater.*, 2015, **377**, 59–64.
3 N. V. Myung, D. Y. Park, B. Y. Yoo, P. T. A. Sumodjo, *J. Magn. Magn. Mater.*, 2003, 265, 189–198.
4 P. C. Andricacos and N. Robertson, *IBM J. Res. Dev.*, 1998, 42, 671–680.
5 Robertson N, Hu B H L and Ching T, *IEEE T. Magn.*, 1997, 33, 2818–2820.
6 Y. Z. Cao, Q. Wang, G. J. Li, J. J. Du, C. Wu and J. C. He, *J. Magn. Magn. Mater.*, 2013, 332, 38–43.
7 L. M. Malkinski, R. Eskandari, A. L. Fogel and S. Min, *J. Appl. Phys.*, 2012, 111, 07A320.
8 T. Kojima, M. Ogiwara, M. Mizuguchi, M. Kotsugi, T. Koganezawa, T. Ohtsuki, T. Tashiro and K. Takanashi, *J. Phys.: Condens. Mat.*, 2014, 26, 064207.
9 A. I. Ustinov, S. S. Polishchuk, S. A. Demchenkov and L. V. Petrushinets, *J. Alloy. Compd.*, 2015, 622, 54–61.
10 T. Shima, M. Okamura, S. Mitani and K. Takanashi, *J. Magn. Magn. Mater.*, 2007, 310, 2213–2214.
11 G. J. Li, Y. Z. Cao, Q. Wang, J. J. Du, Y. Zhao and J. C. He, *Vacuum*, 2014, 106, 75–78.
12 R. Ferrando, J. Jellinek and R. L. Johnston, *Chem. Rev.*, 2008, 108, 845–910.
13 D. H. Kim, H. Y. Kim, H. G. Kim, J. H. Ryu and H. M. Lee, *J. Phys.: Condens. Mat.*, 2008, 20, 035208.
14 M. M. Mariscal, S. A. Dassie and E. P. M. Leiva, *J. Chem. Phys.*, 2005, 123, 184505.
15 G. J. Li, Q. Wang, T. Liu, K. Wang and J. C. He, *J. Clust. Sci.*, 2010, 21, 45–55.
16 F. J. Palacios and M. P. Iniguez, *Nucl. Instrum. Meth. B*, 2002,196, 253–260.
17 C. L. Kuo and P. Clancy, *J. Phys. Chem. B*, 2005, 109, 13743–13754.
18 D. Schebarchov, S. C. Hendy and W. Polak, *J. Phys.: Condens. Mat.*, 2009, 21, 144204.
19 S. C. Lee, N. M. Hwang, B. D. Yu and D. Y. Kim, *J. Cryst. Growth*, 2001, 223, 311–320.
20 J. C. Jiménez-Sáez, A. M. C. Pérez-Martín and J. J. Jiménez-Rodríguez, *Nucl. Instrum.*

Meth. B, 2009, 267, 1447–1450.
21 R. Ge, P. C. Clapp and J. A. Rifkin, *Surf. Sci.*, 1999, 426, L413–L419.
22 G. J. Li, Q. Wang, H. T. Li, K. Wang and J. C. He, *Chinese Phys. B*, 2008, 17, 3343–3349.
23 D. J. Cheng and D. P. Cao, *Chem. Phys. Lett.*, 2008, 461, 71–76.
24 G. J. Li, Q. Wang, D. G. Li, X. Lü and J. C. He, *Phys. Lett. A*, 2008, 372, 6764–6769.
25 G. J. Li, Q. Wang, D. G. Li, X. Lü and J. C. He, *Mater. Chem. Phys.*, 2009, 114, 746–750.
26 H. N. G. Wadley, X. Zhou, R. A. Johnson and M. Neurock, *Prog. Mater. Sci.*, 2001, 46, 329–377.
27 Hugh Baker, *ASM Handbook Volume 3: Alloy Phase Diagrams*, ASM International: Materials Park, Ohio, 1992.
28 Y. Qi, T. Cagin, W. L. Johnson and W. A. Goddard III, *J. Chem. Phys.*, 2001, 115, 385–394.
29 K. K. Nanda, S. N. Sahu and S. N. Behera, *Phys. Rev. B*, 2002, 66, 013208.
30 X. Liu, C. G. Meng and C. H. Liu, *Phase Transit.*, 2006, 79, 249–259.
31 G. J. Li, Q. Wang, Y. Z. Cao, X. Lü and J. C. He, *Acta Phys. Sin.*, 2011, 60, 093601.
32 G. Rossi and R. Ferrando, *Nanotechnology*, 2007, 18, 225706.
33 I. Parsina and F. Baletto, *J. Phys. Chem. C*, 2010, 114, 1504–1511.
34 S. K. R. S. Sankaranarayanan, V. R. Bhethanabotla and B. Joseph, *Phys. Rev. B*, 2005, 71, 195415.
35 J. C. Jiménez-Sáez, A. M. C. Pérez-Martín and J. J. Jiménez-Rodríguez, *Phys. Status Solidi A*, 2008, 205, 1330–1336.